Research Square

Preprints are preliminary reports that have not undergone peer review.
They should not be considered conclusive, used to inform clinical practice,
or referenced by the media as validated information.

Stability analysis of a delayed tuned mass system with hysteretic damping

Khogesh Rathore
Amity University
Saurabh Biswas
saurabh.biswas@iitjammu.ac.in
Indian Institute of Technology Jammu

Research Article

Keywords: Tuned mass damper, Hysteresis, Lyapunov exponent, Galerkin approximation, Harmonic balance method, Multi-frequency approximation

Posted Date: August 28th, 2026

DOI: https://doi.org/10.21203/rs.3.rs-10812877/v1

License: This work is licensed under a Creative Commons Attribution 4.0 International License.
Read Full License

Additional Declarations: No competing interests reported.

Stability analysis of a delayed tuned mass system with hysteretic damping

Khogesh Kumar Rathore[1] and Saurabh Biswas[2]

[1]Amity School of Engineering and Technology, Amity University, Hyderabad, Hyderabad - 500108, Telangana, India .
[2]Department of Mechanical Engineering, Indian Institute of Technology Jammu, Jagti Campus, Jammu, Jammu and Kashmir, 181221, India .

Contributing authors: kkrathore@hyd.amity.edu; saurabh.biswas@iitjammu.ac.in;

Abstract

Tuned Mass Dampers (TMDs) are extensively used in structural and mechanical systems to suppress excessive vibrations by tuning their natural frequency to that of the primary structure. The stability characteristics of TMDs governed by ordinary differential equations have been widely investigated. However, systems incorporating time delays remain relatively unexplored due to their infinite-dimensional characteristics and increased computational complexity. Time delay effects may arise from sensor response times, actuation lags, and control processing. Hysteretic damping, originating from internal material friction and structural nonlinearities, provides a more in-depth representation of energy dissipation in practical applications. In this paper, the dynamic behavior and stability of a delayed tuned mass damper with hysteretic damping are investigated. An asymmetric scalable hysteresis model is adopted to capture nonlinear energy dissipation characteristics. The governing delay differential equations are reduced to a finite-dimensional system using the Galerkin projection method, enables a tractable stability analysis. The coupled effects of time delay and hysteresis on the system response are systematically examined, revealing stability transitions and critical parameter thresholds. The results provide valuable insights into the interaction between delay effects and nonlinear damping, contributing to the design and improved performance of the nonlinear systems in engineering applications.

Keywords: Tuned mass damper, Hysteresis, Lyapunov exponent, Galerkin approximation, Harmonic balance method, Multi-frequency approximation

1 Introduction

The presence of time delays in dynamic systems plays a crucial role in determining their stability and performance. These delays can originate from various sources, including sensor response times, actuator dynamics, and computational processing in real-time control systems [1]. Time delays are particularly significant in engineering applications, where small delays can lead to drastic changes in system behavior, including instability and performance degradation [2]. Early research by Stepan [3] and Hale [4] laid the foundation for analyzing delay-induced instabilities using delay differential equations (DDEs), which are characterized by an infinite number of characteristic roots due to their transcendental nature. Unlike ordinary differential equations (ODEs), stability analysis of DDEs is more complex, as these characteristic roots cannot be expressed in closed form, making analytical solutions challenging. Various numerical approaches developed by Engelborghs et al. [5] and Bellen et al. [6], to directly simulate DDEs, but their computational complexity and dependency on discretization methods have driven interest in alternative strategies. Projection-based techniques, such as the Galerkin approximation, offer a systematic way to transform DDEs into solvable ODE systems, simplifying stability and response analysis. Atay [7] and Michiels and Niculescu [8] explored such stability control methods for complex time-delay systems, improving the theoretical approach for delay-induced dynamics. More recently, Balija et al. [9] studied the stability of a first-order Hayes delay differential equation with scalable hysteresis. By applying the Galerkin projection, stability boundaries were identified, showing the interaction between delay and hysteretic damping. Ospanov [10] also performed stability analysis of linear delay models and demonstrated the existence of periodic solutions. The semi-discretization method introduced by Insperger and Stepan [11] proven to be effective for analyzing time-delay systems in engineering applications.

With increasing interest in time-delayed vibration control systems, the role of delays in application such as Tuned Mass Dampers (TMDs) emerges as a prominent research of focus. TMDs, widely used in mechanical and structural systems, serve as passive vibration control devices designed to suppress excessive vibrations effectively. The concept, introduced by Frahm [12] in the early 20th century, theoretically developed by Den Hartog [13], formulated tuning principles to optimize vibration reduction. Modern advancements have introduced variations such as hybrid and adaptive TMDs (see [14–17]), allow real-time adjustments to external excitations. However, the introduction of delay in TMD systems presents both challenges and opportunities, as it can lead to stability concerns while also offering improved tunability. The delay inclusion in vibration control mechanisms are of great interest of study in structural applications. Jian and Ou [18] explored time delay compensation methods in active Tuned Mass Damper (TMD) systems, demonstrating improvements in system stability through predictive control. Zhao et al. [19] examined the effects of time delays in semi-active TMD systems, identifying critical delay thresholds for stability under different operating conditions. Studies such as those by Gebrial and Sinan [20] examined mass ratio factors for optimized TMD strategies, further refining the design of these control devices.

The inclusion of non-linear damping mechanisms, such as hysteresis, influences the real performance of delayed TMD systems. Hysteresis, characterized by energy dissipation due to material nonlinearity and internal friction, is widely studied. Early observations by Rowett [21] highlighted its role in cyclic loading, leading to the development of mathematical models such as the Preisach and Iwan models [22, 23]. The Bouc-Wen model [24, 25] remains one of the most popular due to its ability to capture various hysteretic behaviors. Despite its versatility, traditional hysteresis models struggle to accurately depict minor loading-unloading loops. To address this, Biswas and Chatterjee [26] introduced an enhanced symmetric hysteresis model motivated by the behavior of elastic plates with frictional micro-cracks. Rathore and Biswas [27, 28] later implemented this hysteresis damping model in TMDs, using numerical and semi-analytical approaches to study the dynamic response.

More recently, an asymmetric hysteresis model was developed by Rathore and Biswas [29], extending the symmetric model to capture a broader range of hysteresis loops, including minor loops arising from partial loading and unloading. The governing equation for this asymmetric hysteresis model is given as:

$$\dot{\theta} = \frac{\kappa}{|x| + \epsilon} \left(A + \theta_a \operatorname{sgn}(\dot{x}) + \beta \operatorname{sgn}(x\dot{x}) - \theta\right) \cdot |\dot{x}|, \tag{1}$$

where θ is an internal variable, x is the input, and the parameters A and β define the model characteristics. The regularization parameter ϵ prevents singularities at $x = 0$. The corresponding hysteretic force output is given by:

$$f = \theta |x|^{\alpha} \operatorname{sgn}(x), \tag{2}$$

where α is a positive parameter controlling the shape of the hysteresis loop.

Incorporating asymmetric hysteresis into a delayed TMD system presents unique challenges and advantages. The delay transforms the governing equation into a transcendental equation, leading to an infinite number of roots that influence system stability. While the TMD provides stability through damping, the presence of delay introduces potential instability but also helps to define stable regions precisely. This study aims to conduct a comprehensive stability analysis of a delayed tuned mass hysteretic damper system, incorporating both non-linear hysteresis and time delay effects. Using Galerkin projection, we transform the governing DDEs into ODEs for stability analysis. The periodic solutions are investigated using numerical arc-based continuation method. The branch periodic solution are investigated using single frequency harmonic balance. Additionally, we employ a multi-frequency approximation to verify periodic solutions on the stability boundaries. The insights gained from this research will contribute to the optimization of TMD systems for enhanced vibration control in real-world engineering applications.

2 Tuned mass damper system with time delays

Figure 1 represents a tuned mass damper (TMD) system, where m_1 represents the mass of the primary structure, which is supported by a spring stiffness K_1. A secondary mass m_2 is attached to the primary mass, connected via a spring of stiffness K_2 and a hysteretic damper denoted by f. The primary mass m_1 is subjected to a harmonic

force $F_0 \sin \omega t$, where F_0 is the amplitude and ω is the angular frequency of the applied force.

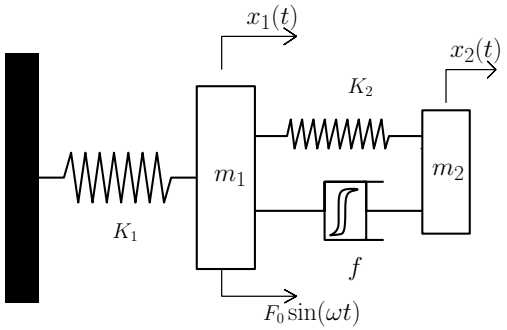


Fig. 1 A tuned mass system with hysteretic damper.

Governing equations of motion of the system are as follows,

$$m_1 \ddot{x}_1(t) + (K_1 + K_2)\, x_1(t) - K_2 x_2(t) - f = F_0 \sin(\omega t), \tag{3}$$

$$m_2(t)\ddot{x}_2 - K_2 x_1(t) + K_2 x_2(t) + f = 0. \tag{4}$$

Here, the hysteretic force

$$f = \gamma \cdot \theta \cdot (x_2(t) - x_1(t))\,, \tag{5}$$

where γ is a scaling factor and θ is an internal state variable given by,

$$\begin{aligned} \dot{\theta} = \frac{\kappa}{|x_2(t) - x_1(t)| + \epsilon} \{A + \theta_a \operatorname{sgn}(\dot{x}_2(t) - \dot{x}_1(t)) \\ + \beta \operatorname{sgn}\left((x_2(t) - x_1(t))(\dot{x}_2(t) - \dot{x}_1(t)) - \theta\right)\} \cdot |\dot{x}_2(t) - \dot{x}_1(t)| \end{aligned} \tag{6}$$

The parameters κ, A, θ_a, and β define the model, and $\epsilon \ll 1$ is a small regularization parameter used to address the singularity at zero input. The hysteretic output is given by

$$f_{hys} = \theta |x|^{\alpha} \operatorname{sgn}(x). \tag{7}$$

Here, α is a positive number.

Now we introduce a unit delay term in Eq. 3 as

$$m_1 \ddot{x}_1(t) + (K_1 + K_2)\, x_1(t) - K_2 x_2(t) - f + \alpha D(t-1) = F_0 \sin(\omega t). \tag{8}$$

Equation 8 is a delay differential equation (DDE). Equation 8 is further transformed into a system of ordinary differential equations using Galerkin projection method as in [9]. We briefly discuss the method for completeness.

The method involves defining the instantaneous time-dependent variable t and the delay variable s using the local function $F(t, s)$ [9]:

$$F(t, s) = Z_s = Z(t - s). \tag{9}$$

The delay is normalized to unity, allowing s to vary from 0 to 1. This normalization simplifies analysis and enhances clarity. The function $F(t, s)$ is approximated as:

$$F(t,s) = a_0(t) + a_1(t)s + \sum_{k=1}^{N-2} a_{k+1}(t)\sin(k\pi s) \tag{10}$$

with state variables $a_0(t), a_1(t), \ldots, a_{N-1}(t)$ and N is the number of shape functions. We consider $N = 15$ for our calculations. The state variables are formulated as:

$$x_1(t) = a_0(t), \quad \dot{x_1} = b_0(t), \quad x_2(t) = c_0(t), \quad \dot{x_2} = a_{N+1}(t)$$

Using the Galerkin projection method [9], the residual formulation is:

$$R(t,s) = \int_0^s \left(\frac{\partial F}{\partial t} + \frac{\partial F}{\partial s}\right) \mathrm{d}s \tag{11}$$

The resulting system of $2N$ equations is numerically integrated using MATLAB's `ode45`.

To validate the results obtained from the Galerkin approximation, we compare the solutions obtained using `ode45` with those, computed using MATLAB's DDE solver, `dde23`, with a tolerance of 10^{-4} for both methods. As a result, all subsequent solutions for Equations 3 and 4 are derived using this method.

Table 1 TMD system parameters considered for stability analysis.

Case	m_1	m_2	K_1	K_2	A	κ	θ_a	β	ϵ
1	1	0.05	1	0.05	3	4	2	1.8	10^{-6}
2	1	0.065	1	0.065	3	4	2	1.8	10^{-6}
3	1	0.1	1	0.1	3	4	2	1.8	10^{-6}
4	1	0.2	1	0.2	3	4	2	1.8	10^{-6}

We compute the solutions for the parameters of Case 1, as shown in Table 1, using both MATLAB's `ode45` and `dde23` solver for the Galerkin approximation method and delay differential equations, respectively. The solutions are calculated for different initial conditions, and varying levels of damping, including both weak and strong damping cases. The results, which compare the outputs from both methods, are illustrated in Figure 2. The result is shown for the first mode of the state variables (i.e. a_0).

The comparison in Figure 2 illustrates that the solutions generated by the Galerkin method align closely with those from dde23, under various parameters and initial states. This strong agreement across different conditions reinforces the validity and accuracy of the Galerkin approximation as an effective approach for solving delay differential equations, particularly in capturing the dynamics introduced by the delay

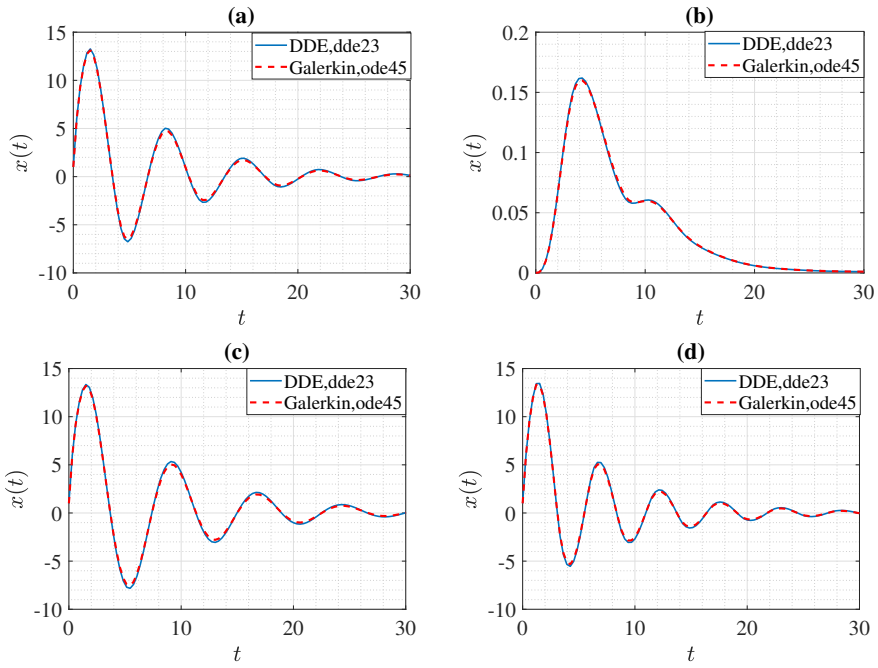


Fig. 2 Displacement vs. time plot for the TMD system with hysteretic damper and unit delay: $m_1 = 1$, $m_2 = \frac{1}{20}$, $K_1 = 1$, $K_2 = \frac{1}{20}$, $A = 3$, $\kappa = 4$, $\theta_a = 2$, $F_0 = 1.2$, $\beta = 1.8$, $\omega = 0.1$, $\epsilon = 1 \times 10^{-6}$ with (a) Non-zero initial conditions ($\gamma = 0.3$) (b) Zero initial conditions ($\gamma = 0.3$) (c) Weak damping ($\gamma = 0.01$) (d) Strong damping ($\gamma = 1$).

term. Consequently, the Galerkin method proves to be a robust alternative for analyzing delay-related phenomena in complex systems. All state variables correspond to Case 1 are shown in Figure 3.

We now study the stability of the system in the next section.

3 Stability Analysis

To examine the stability of the system defined by Eq. 8, we start by generating stability regions using exhaustive numerical solutions on a grid. This process adopts a Lyapunov-like exponent to analyze stability. To enhance the computational efficiency, we used the finite-dimensional approximations of the delay differential equation. This numerical method implemented for Lyapunov-like exponent, executed in [9], used to analyze the stability of non-linear systems, with hysteresis.

To investigate the influence of delay coupled with hysteretic damping on the system's stability, we initially conduct a stability analysis with the parameters, as presented in Table 1. We examine stability of the system under different damping conditions: zero damping ($\gamma = 0$), weak damping ($\gamma = 0.3$) and strong damping ($\gamma = 1$). The analysis focuses on identifying the stable (bounded) regions in the parameter space. Given the analytical complexity of the nonlinear forced system, some solutions remain bounded while others exhibit unbounded growth depending on the parameter

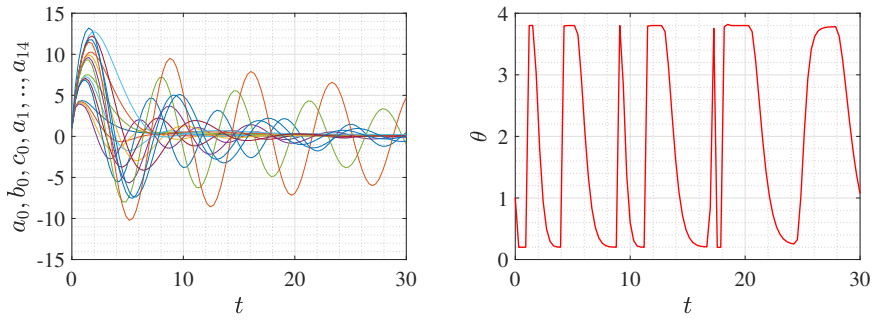


Fig. 3 (Left): All state variables are plotted against time of the TMD system with hysteretic damper and unit delay using Galerkin approximation. The parameters with unit delay are: $m_1 = 1$, $m_2 = \frac{1}{20}$, $K_1 = 1$, $K_2 = \frac{1}{20}$, $A = 3$, $\kappa = 4$, $\theta_a = 2$, $F_0 = 1.2$, $\beta = 1.8$, $\omega = 0.1$, $\epsilon = 1 \times 10^{-6}$.(Right): θ against t.

values. Specifically, unbounded (unstable) solutions grow exponentially. To understand this behavior, we analyze their exponential growth rates using a Lyapunov-like exponent. This evaluation provides deeper insight into the transition between delay, hysteretic damping, and system stability.

3.1 Lyapunov-like exponent

To begin, we define the Lyapunov-like exponent as

$$\lambda = \lim_{M \to \infty} \frac{1}{M} \sum_{k=0}^{M} \ln \left(\left\| Z_k^{\mathrm{T}} \right\| \right), \tag{12}$$

In computations, a large but finite value of M will be used, with Z representing the scalable portion of the state vector. The subscript k in Z_k^T denotes the step number in the calculation, while the superscript (either 0 or T) indicates the start or end of a step, respectively. The calculation progresses step by step as follows.

We integrate the governing equations over the interval from 0 to T, starting with randomly chosen, unit-normalized initial conditions Z_0^0. After first integration, we have end state vector as Z_0^T, for the next integration step the initial conditions are evaluated by normalizing Z_0^T as:

$$Z_1^0 = \frac{Z_0^T}{|Z_0^T|}$$

By integrating over an additional time step, we obtain Z_1^T. This process is repeated for M time steps, allowing us to approximate λ using a large but finite M (here, $M = 450$). For a selected point in the parameter space, a positive λ (i.e., $\lambda > 0$) indicates average exponential growth, suggesting that the system is unstable. Stability is inferred when $\lambda < 0$. In our computations, we consider the system unstable when λ exceeds a small positive threshold, chosen here as 10^{-3}. The Lyapunov-like exponent of the Tuned mass hysteretic damper system with delay is presented in the Figure 4. The plot illustrates the analysis based on the cases and parameters provided in Table 1.

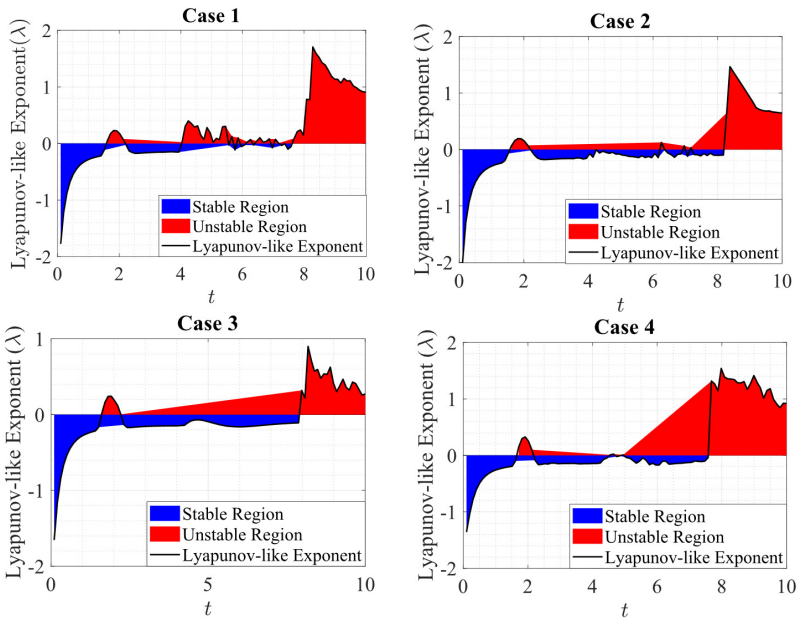


Fig. 4 Lpapunov-like exponent stability chart for cases of Table 1. Blue region: Stable; Red region: Unstable.

We now observe Lyapunov-like exponents indicating stable and unstable regions. The plot shows Lyapunov-exponent (λ), of the normalized state variables from Galerkin's approximation for stable region ($\lambda < 1$) and unstable region ($\lambda > 1$). For each $M = 450$, there exists λ either positive or negative. Now, the stable and unstable area are of our interest. To better understand the stability and enhance our findings, we generate a stability chart for the Galerkin-approximated equations in variations of m_2 and K_2 values, as detailed in Table 1. For each combination of m_2 and K_2, the corresponding eigenvalues (λ) are determined in their stable and unstable forms. We note that the damping ratio ($\gamma = 0.3$) opted for the Lyapunov stability study.

3.2 Stability charts

Following the Lyapunov-based stability analysis, stable and unstable regions were identified with respect to λ. To further explore the influence of primary mass (m_1) and stiffness (K_1) on system stability, a parametric study is performed by systematically varying m_1 and K_1. This analysis is extended across different secondary mass-stiffness combinations (m_2, K_2), as listed in Table 1, and under three damping cases: $\gamma = 0$, $\gamma = 0.3$, and $\gamma = 1$.

Cases 1 and 2 in Table 1 correspond to optimal tuning conditions from [20], adhering to practical mass ratios ($m_{\text{tmd}}/m_{\text{p}} < 0.1$), while cases 3 and 4 are chosen to examine broader stability behavior. Stability charts in Figure 5 illustrate regions of $\lambda < 1$ (stable, blue) and $\lambda > 1$ (unstable, green), highlighting damping-induced shifts in stability boundaries.

Zero damping ($\gamma = 0$) yields larger stable regions (cases 1a, 2a, 3a), though such conditions are impractical due to the absence of energy dissipation. As damping increases, particularly at $\gamma = 0.3$ in case 3b, instability becomes more prominent, emphasizing the dual role of damping in both stabilizing and destabilizing system dynamics. These results demonstrate the complex interaction between damping, mass, stiffness, and hysteretic effects in defining the system's stability.

Among all four configurations and damping levels considered, case 1b yields the most favorable stability performance. This is primarily due to the use of optimal TMD tuning ratios and well-selected hysteretic parameters, which together ensure effective vibration mitigation. These parameters are thus adopted as a reference throughout the remainder of the study.

We note that, the cases 1c, 2c, and 3c show instability at $\gamma = 1$. Despite consistent hysteretic parameters, variations in m_1 and K_1 under high damping introduce overdamped behavior. This leads to delayed TMD response, limited energy transfer, and the amplification of energy due to combined delay and hysteresis effects.

Case 4a, characterized by a non-optimal TMD ratio and absence of damping, exhibits substantial instability. The system's inability to absorb vibrations under such configurations results in uncontrolled oscillations. Introduction of damping in case 4b enhances stability, though increased γ introduces slower response and higher dissipation. In case 4c, the combination of high damping and a deviated TMD ratio results in complex and chaotic dynamics, yet identifiable pockets of stability remain, offering insight into operational regimes.

Previously, the stability analysis varied m_1 and K_1 over a fixed set of secondary parameters. Now the current study reverses this approach by fixing m_1 and K_1 for each case and examining system stability over a range of m_2 and K_2 values. This complementary analysis, performed for $\gamma = 0$, 0.3, and 1, broadens understanding of the stability boundaries. The results are illustrated in Figure 6, and the corresponding parameters are listed in Table 2.

The stability of the delayed tuned mass damper (TMD) system with hysteretic damping is analyzed for varying secondary mass (m_2) and stiffness (K_2) under three damping levels ($\gamma = 0$, 0.3, and 1), as shown in Figure 6. The analysis considers four cases with different primary mass-stiffness pairs (m_1, K_1), listed in Table 2. The parameters used for the analysis are presented in Table 2.

Table 2 TMD system parameters considered for stability analysis.

Case	m_1	K_1	A	κ	θ_a	β	ϵ
1	0.4	0.4	3	4	2	1.8	10^{-6}
2	0.8	0.8	3	4	2	1.8	10^{-6}
3	1.2	1.2	3	4	2	1.8	10^{-6}
4	1.6	1.6	3	4	2	1.8	10^{-6}

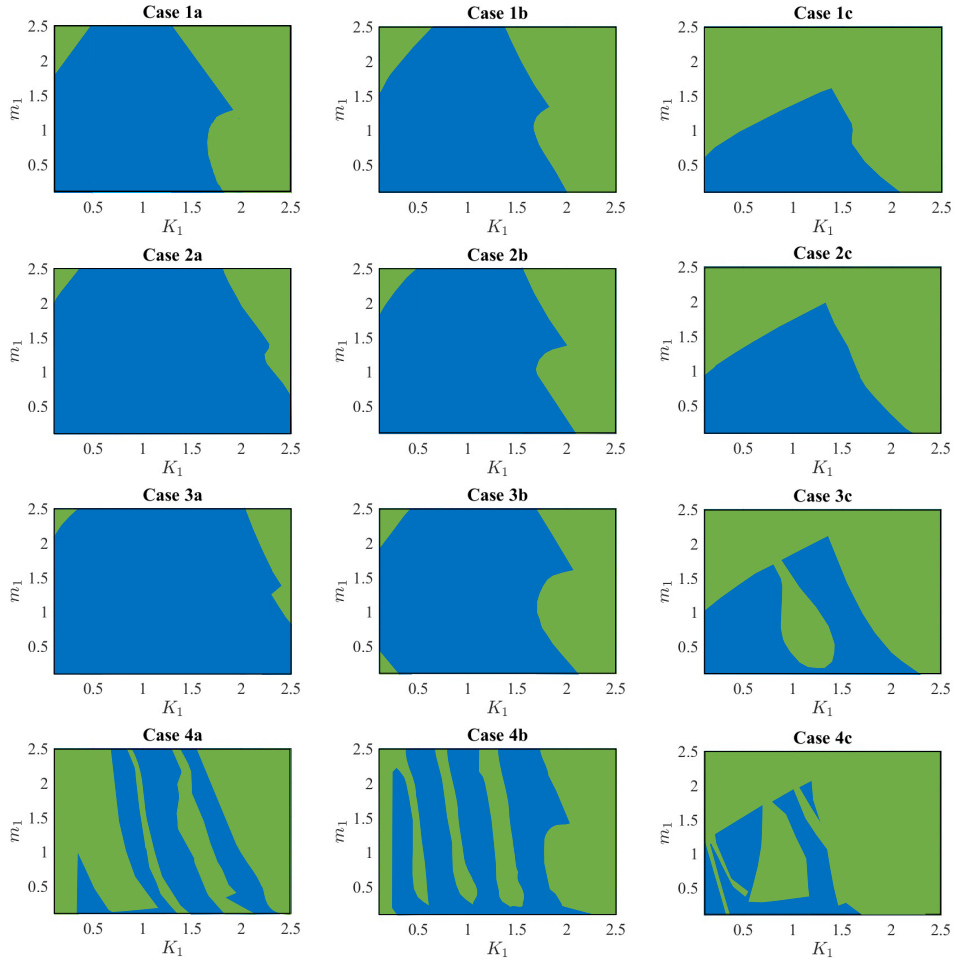


Fig. 5 Stability chart of the tuned mass hysteretic damper system with delay for all the cases presented in Table 1, evaluated for different damping parameter values γ: (a) 0; (b) 0.3; (c) 1. The blue region represents stability, while the green region indicates instability.

In the undamped scenario ($\gamma = 0$), cases 1a through 4a exhibit widespread instability, with negligible stable regions due to the dominance of delay and hysteretic effects. Introducing moderate damping ($\gamma = 0.3$) expands stability regions, notably in case 4b, indicating improved resilience to delay effects with increased m_1 and K_1. However, for lower m_1, stability remains limited. At high damping ($\gamma = 1$), cases 1c through 4c display broader stability across all parameter ranges, although excessive damping may counteract hysteretic benefits and induce instability.

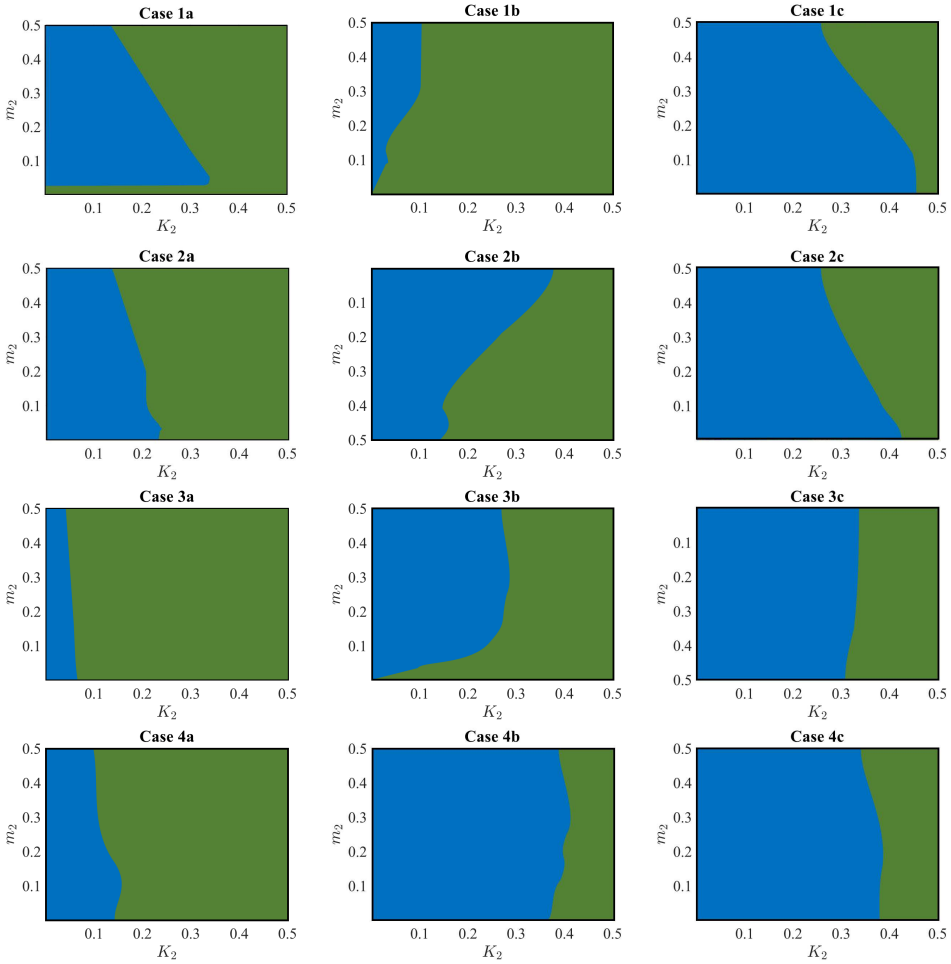


Fig. 6 Stability chart of the tuned mass hysteretic damper system with delay for all the cases presented in Table 2, evaluated for different damping parameter values γ: (a) 0; (b) 0.3; (c) 1. The blue region represents stability, while the green region indicates instability.

To further validate the stability chart, four representative coordinates are selected from the stable and unstable regions of case 1b (see Figure 7). The corresponding displacement responses are shown in Figure 8. Plots in Figure 8(a), (b), (c) and (d) corresponds to Point 1, 2, 3 and 4. Figure 8(a) and (b) exhibit divergent and periodic responses respectively, both within the unstable domain, while 8(c) and (d) show convergent behavior from the stable region.

Notably, Point 2 in Figure 8(b) demonstrates a periodic solution at the stability boundary, marking the transition between stable and unstable regimes. This critical point is further investigated in the next section to analyze the system's dynamic response at the stability threshold.

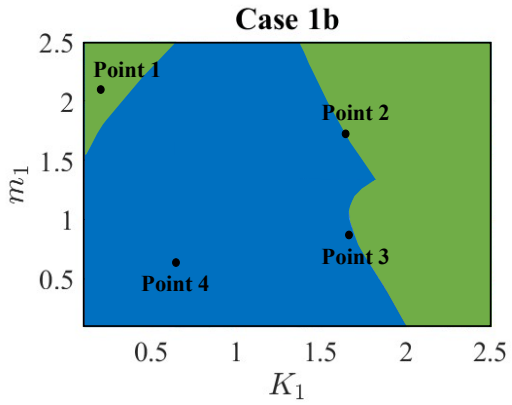


Fig. 7 Stability chart of Case 1b paramters with random selected four points. Point 1 ($K_1 = 0.221$, $m_1 = 2.12$), Point 2 ($K_1 = 1.67$, $m_1 = 1.87$), Point 3 ($K_1 = 1.62$, $m_1 = 0.73$), Point 4 ($K_1 = 0.671$, $m_1 = 0.683$)

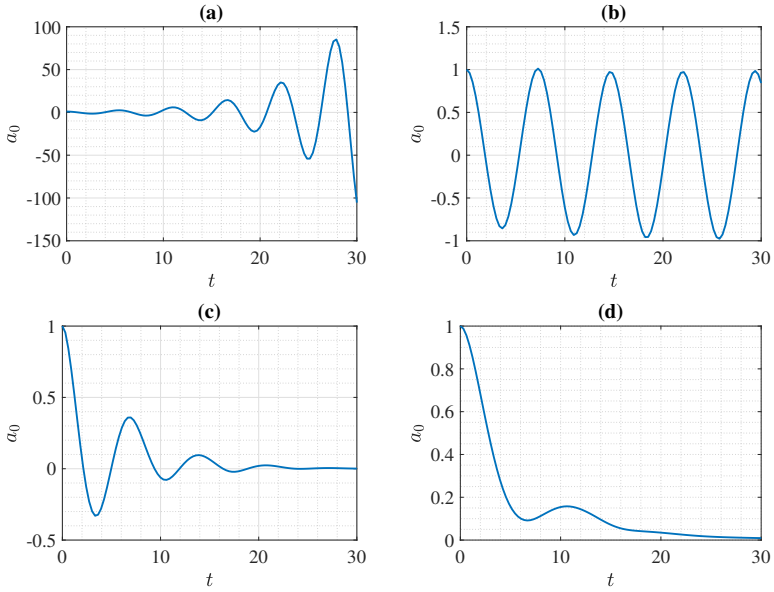


Fig. 8 Displacements plots of the selected points of case 1b as shown in Figure 7, with parameters (left): $m_1 = 1; m_2 = 1/5; K_1 = 1; K_2 = 1/5;\ A = 3;,\ \kappa = 4;\ \theta_a = 2;\ F_0 = 1.2; \omega = 0.1; \gamma = 0.3; \beta = 1.8; \epsilon = 1e-6$.

4 Periodic solution on the stability boundary

The periodic solutions typically occur at the transition between stable and unstable boundaries. We will investigate the boundary regions where periodic solutions may

arise. To compute the periodic solution at the stability boundary, we refer to the stability chart of case 1b and 2b shown in the Figure 5.

We apply a numerical arc-length-based continuation method [9] to trace the periodic curve for the same range of m_1 and K_1. The arc-length continuation is a powerful numerical method used to trace solution branches of nonlinear equations or systems, especially when conventional methods fail near turning points or bifurcations. It is widely applied in the analysis of nonlinear dynamical systems.

To brief we consider a system of equations:

$$f(x;\mu) = 0, \tag{13}$$

where x is the solution vector (here displacement), and μ is the frequency.

When the parameter μ is varied, the solutions form a continuous curve in x-space. Traditional continuation techniques increases μ and rely on the previous solution as the initial guess for the next step. However, these methods encounter difficulties at turning points or bifurcations, where the curve changes direction.

The core idea of an arc-length continuation is instead of treating μ as an independent parameter, we consider both x and μ as variables and enforce a constant arc-length step along the solution curve. This ensures that the continuation process does not break down at turning points. The solution curve is parameterized by the arc-length s, and the system can reformulated as:

$$f(x;\mu) = 0,$$

$$\|(x,\mu) - (x_{\text{previous}}, \mu_{\text{previous}})\| - s = 0,$$

where s is the step size, and $(x_{\text{previous}}, \mu_{\text{previous}})$ is the previous solution.

Now, we introduce the augmented variable $y = [x;\mu]$, combining the solution vector x and parameter μ. The augmented system becomes:

$$F(y) = \begin{bmatrix} f(x;\mu) \\ \|y - y_{\text{previous}}\| - s \end{bmatrix} = 0.$$

This system has as many equations as variables, enabling it to be solved numerically. Using previously computed solutions y_0 and y_1 to extrapolate an initial guess y_g for the next solution:

$$y_g = 2y_1 - y_0$$

We now apply Newton-Raphson iterations to solve the augmented system $F(y) = 0$

$$y_{k+1} = y_k - J^{-1}F(y_k),$$

Here, $F(y)$ is the augmented system. J is the Jacobian matrix of F with respect to y. Once the system converges to a solution $y_{new} = [x_{new};\mu_{new}]$, We update the augmented variable and repeat the process to trace the entire curve.

In our analysis of the periodic solutions within the stable and unstable boundary, we consider the resulting equations derived from the Galerkin projection, including

the damping equation. These equations are augmented with the parameter μ and collectively form the system.

The results of the periodic solution for cases 1b and 2b, with incremental changes in the parameters x and μ, are presented in Figure 9. There can be branches of the periodic solutions along the periodic solution curve (discussed later).

We note that the periodic solution obtained tend towards the decreasing K_1 values as the m_1 increases. This trend indicates a growing instability in the system, as the periodic solution struggles to maintain coherence under these changing conditions. The drift visible at $m_1 = 1.4121$ and $K_1 = 1.7411$, encounter numerical challenges in accurately capturing the curves at points. To facilitate a more detailed investigation of the periodic solution, five specific points, labeled P1 through P5, is marked in Figure 9(a). These points will serve as key reference locations for a deeper analysis of the systems behavior across different parameter values.

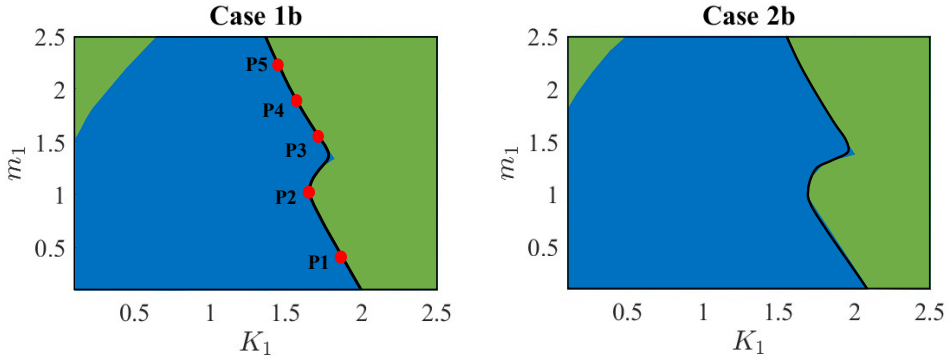


Fig. 9 Periodic solution for tuned mass hysteretic damper system with delay, for parameters (left): $m_1 = 1; m_2 = 1/5; K_1 = 1; K_2 = 1/5; F_0 = 1.2; \omega = 0.1; \gamma = 0.3; \beta = 1.8; \epsilon = 1e-6$. (right): $m_1 = 1; m_2 = 1/10; K_1 = 1; K_2 = 1/10; F_0 = 1.2; \omega = 0.1; \gamma = 0.3; \beta = 1.8; \epsilon = 1e-6$. Black region: Periodic solution; Blue region: Stable; Green region: Unstable.

Figure 10 illustrates the time evolution of a_0(t) versus time t for one complete cycle of oscillation, as observed at each of the points P1 through P5. A clear trend of decreasing amplitude, steady state and increasing time period is evident as the oscillation progresses, highlighting the gradual changes in the system's dynamics due to the rate-independent hysteresis. The amplitude of a_0 decreases as m_1 increase and K_1 decreases, which logically supports the findings of our study.

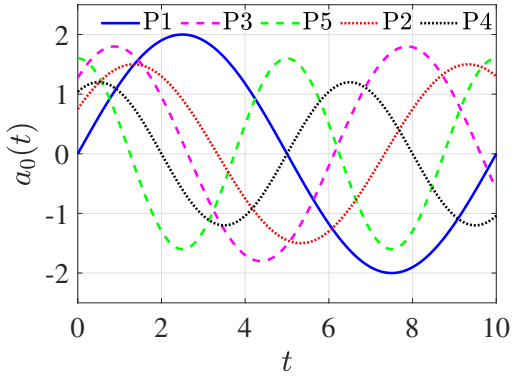


Fig. 10 Numerical solutions for a_0(t) against t, for points P_1 through P_5. Parameters: N =14, A = 3, $\kappa = 4$, $\theta_a = 2$, $\beta = 1.8$, $\gamma = 0.3$.

It is noteworthy that the higher state variables exhibit small-amplitude, high-frequency oscillations, which pose challenges for numerical analysis. These high-frequency fluctuations can make it difficult to obtain accurate numerical results, as they introduce instability or excessive computational noise, complicating the process of capturing the system's true behavior. Now, we approach an alternate way for numerical continuation to study the difference in the characteristic behavior with two methods i.e. (a) Single frequency harmonic balance method to capture the branches of periodic solution and (b) Multi-frequency approximation.

4.1 Single-frequency harmonic balance

Single-frequency harmonic balance is a semi-analytical approach for solving nonlinear differential equations that govern the behavior of oscillating systems. The technique assumes that the system's response can be approximated as a sum of sinusoidal waves, each corresponding to a different frequency. It is employed to study the branch of periodic solution of systems that experience periodic or oscillatory responses under the influence of nonlinearities [39]. We discuss the approach .

We assume unit amplitude for the system as,

$$x_1(t) = X_1 \sin(\omega t + \phi - 1) \quad \text{and} \quad x_2(t) = X_2 \cos(\omega t + \phi - 1). \tag{14}$$

We approximate the hysteretic response of Eq. 6 for input $\sin \omega t$ input as,

$$\theta(t) z(t) \approx \alpha_0 \ \sin \omega t + \alpha_1 \ \cos \omega t. \tag{15}$$

To determine the coefficients α_0 and α_1, we fit these values from numerical solutions obtained using the hysteresis model. For the chosen parameters of the hysteresis model the $\alpha_0 = 4.1244$ and $\alpha_1 = 0.7693$ are obtained. These values are independent of the frequency ω because the hysteresis is rate-independent.
Substituting Eqs. 14 and 15 in Eqs. 3 and 4, then setting the coefficients to zero, we

obtained the following two equations

$$-m_1 X_1 \sin(\omega t + \phi_1 - 1)\omega^2 + (K_1 + K_2)X_1 \sin(\omega t + \phi_1 - 1) - K_2\big(X_2 \cos(\omega t + \phi_1 - 1) - Z \sin(\omega t)\big) + \gamma\big(\omega_0 \sin(\omega t) + \alpha_1 \cos(\omega t)\big) - F \sin(\omega t + \phi_2) = 0 \tag{16}$$

$$-m_2 X_2 \cos(\omega t + \phi_1 - 1)\omega^2 + (K_2)X_1 \sin(\omega t + \phi_1 - 1) - K_2\big(X_2 \cos(\omega t + \phi_1 - 1) + Z \sin(\omega t)\big) + \gamma\big(\omega_0 \sin(\omega t) + \alpha_1 \cos(\omega t)\big) - F \sin(\omega t + \phi_2) = 0 \tag{17}$$

Equations 16 and 17 are solved with ω as a parameter. We obtain the branches of periodic solution for the Cases 1b and 2b. The results are presented in Figure 11 alongside the periodic solution obtained through numerical continuation.

In Figure 11, periodic solution branch captures the curve near the coordinate points $m_1 = 1.4121$ and $K_1 = 1.7411$ in Case 1b and $m_1 = 1.4342$, $K_1 = 2.0021$ in Case 2b and $m_1 = 1.5732$, $K_1 = 2.241$ effectively. This is likely because the harmonic mean values were used to approximate the curves. The match is consistent over a broad region, validating the numerical evidence for the existence of periodic solutions. A more precise approximation for multiple frequencies is outlined in the next section.

4.2 Multi-frequency approximation

We apply a numerically-assisted multi-frequency approximation technique to describe the periodic solution branch [27]. This method is applicable when the solution develops harmonics without small rate reversals. It exploits the scalability and time-invariance of the hysteresis model. Consequently, for approximating the hysteretic force, we begin with a unit amplitude and replace the actual time with a distorted time.

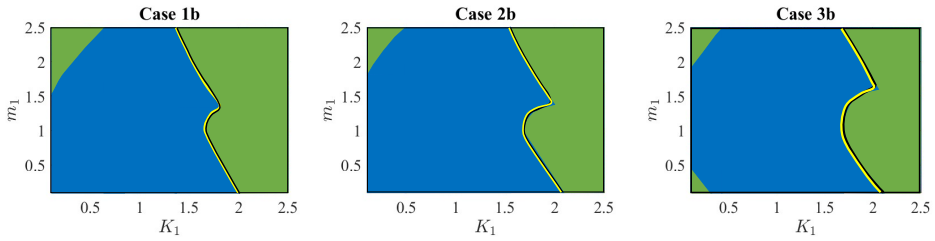


Fig. 11 Stability chart of Cases 1b, 2b and 3b. Black curve: periodic solutions by numerical continuation. Yellow curve: Branched periodic solution obtained by HBM.

We begin with our hysteresis model

$$\dot{\theta} = \frac{\kappa}{|x| + \epsilon}\{A + \theta_a \operatorname{sgn}(\dot{x}) + \beta \operatorname{sgn}(x\dot{x}) - \theta\} \cdot |\dot{x}|. \tag{18}$$

To approximate the hysteretic response, we introduce a new distorted timescale.

$$\tau = \omega t + \sum_{k=1}^{\pi} [A_k \sin k\omega t + B_k(\cos k\omega t - 1)] \tag{19}$$

where ω represents the fundamental frequency. It is important to note that $\tau = 0$ when t = 0. Assuming solutions

$$x_1 = A\sin(\tau + \phi_1) \tag{20}$$
$$x_1 - x_2 = B\sin\tau \tag{21}$$

and the applied external force as

$$F = F_0 \sin(\tau + \phi_2) \tag{22}$$

Here ϕ_1 and ϕ_2 are the phases. The hysteretic response is approximated as follows:

$$\theta(\tau)x(\tau) \approx \alpha_0 \sin\tau + \alpha_1 \cos\tau + \alpha_2 \sin 3\tau + \alpha_3 \cos 3\tau \tag{23}$$

The coefficients α_0 through α_3 are determined by fitting them to numerical solutions. For the selected parameters of the hysteresis model, the values are found to be $\alpha_0 = 3.125$, $\alpha_1 = 0.7638$, $\alpha_2 = -0.5625$, and $\alpha_3 = -0.3829$.

By substituting Eq. 19 into Eqs. 20 through 22, we obtain:

$$x_1 = A\sin\left(\omega t + \sum_{k=1}^{n} [A_k \sin k\omega t + B_k(\cos k\omega t - 1)] + \phi_1\right) \tag{24}$$

$$x_1 - x_2 = B\sin\left(\omega t + \sum_{k=1}^{n} [A_k \sin k\omega t + B_k(\cos k\omega t - 1)]\right) \tag{25}$$

and,

$$\begin{aligned}\theta(t)x(t) \approx\ & \alpha_0 \sin\left(\omega t + \sum_{k=1}^{n} [A_k \sin k\omega t + B_k(\cos k\omega t - 1)]\right) \\ & + \alpha_1 \cos\left(\omega t + \sum_{k=1}^{n} [A_k \sin k\omega t + B_k(\cos k\omega t - 1)]\right) \\ & + \alpha_2 \sin\left(3\omega t + \sum_{k=1}^{n} [3A_k \sin k\omega t + 3B_k(\cos k\omega t - 1)]\right) \\ & + \alpha_3 \cos\left(3\omega t + \sum_{k=1}^{n} [3A_k \sin k\omega t + 3B_k(\cos k\omega t - 1)]\right)\end{aligned} \tag{26}$$

Substituting Eqs. 25 and 26 into the delay differential equation (Eqs. 3 and 4), we derive a lengthy analytical expression for the residual, which depends on X_1, ϕ_k, A_k^s, B_k^s, ω and t (details skipped). This expression is referred to as the residual.

$$\bar{R}(X_1, Z, \mathbf{A}, \mathbf{B}, \omega, t),$$
$$\mathbf{A} = A_1, A_2, \ldots, A_n; \quad \mathbf{B} = B_1, B_2, \ldots, B_n$$

We then minimize $\bar{R}$ in the least squares sense to derive a total of $2n+2$ equations, as shown below. For the minimization, we proceed by taking:

$$\frac{\partial}{\partial X_1} \int_0^{2\pi/\omega} \bar{R}^2 \, \mathrm{d}t = \int_0^{2\pi/\omega} \bar{R} \frac{\partial \bar{R}}{\partial X_1} \, \mathrm{d}t = 0 \tag{27}$$

Similarly, we have

$$\int_0^{2\pi/\omega} \frac{\partial R}{\partial \phi_k} \, \mathrm{d}t = 0, \tag{28}$$
$$\int_0^{2\pi/\omega} \bar{R} \frac{\partial \bar{R}}{\partial A_k} \, \mathrm{d}t = 0, \quad k = 1, \ldots, n, \tag{29}$$
$$\int_0^{2\pi/\omega} \bar{R} \frac{\partial \bar{R}}{\partial B_k} \, \mathrm{d}t = 0, \quad k = 1, \ldots, n. \tag{30}$$

We found that $n = 2$ is sufficient. Therefore, we obtain a system of six equations with six unknowns: X_1, ϕ_k, A_1, A_2, B_1 and B_2, while ω remains a free parameter. The integrals are evaluated numerically using Simpson's rule with a high resolution (850 points). Equations 27 through 30 are solved iteratively using the Newton-Raphson method, with numerically estimated Jacobians and a tolerance of 10^{-5}. Figure 12 illustrates the periodic solution branch (in red), which was obtained by solving Equations. 27 through 30. Figure 12 presents all case 1b, 2b, 3b and 4b plots obtained using all methods as mentioned. It is noteworthy that the solution matches closely with the numerically determined stability boundary using Lyapunov-like exponents on a grid, as well as the numerically obtained periodic solutions where the continuation method faced challenges.

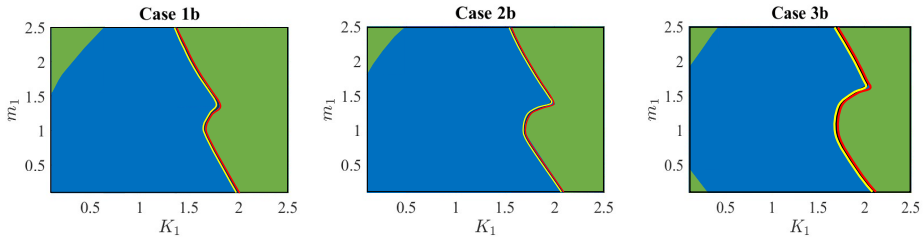


Fig. 12 Stability chart of Case 1b, 2b and 3b. Black curve: periodic solutions by numerical continuation. Yellow curve: Periodic solution branch obtained by Single frequency harmonic balance. Red curve: Periodic solution obtained from a multi-frequency approximation.

5 Conclusion

In this study, we conducted a comprehensive exploration of the stability characteristics and transition boundaries of a tuned mass damper (TMD) system that incorporates both time delay and an asymmetric hysteresis model. The governing equations for this system include a differential equation with scalable hysteresis, allowing for a more generalized representation of damping effects. It is well known that the presence of time delay in dynamical systems can significantly amplify instability. However, to the best of our knowledge, no prior research has systematically investigated this specific combination of delay, hysteresis, and stability criteria in TMD systems. Our study leads to novel insights into the complex interactions governing the system's behavior.

A key aspect of our approach is the scalability of the hysteretic force to employ Lyapunov-like exponents for stability analysis. While these exponents do not directly quantify the stability of individual trajectories, they offer deep insights to the average exponential growth rates of system responses, thereby providing a broader perspective on stability transitions. This analytical approach enabled us to uncover complex behaviors resulting from the relation between stable and unstable solution regions.

Among the most significant findings was the identification of periodic solutions emerging along transition boundaries. These phenomenon highlights the intricate balance between stability and instability, influenced by the combined effects of hysteresis and delay. The numerical challenges associated with computing periodic solutions using traditional continuation methods prompted us to explore an alternative multi-frequency approximation technique. While inspired by harmonic balance principles, this novel approach deviates in its formulation, offering a more tractable yet effective means of approximating periodic solutions. The solutions obtained through this approximation are successfully visualized and demonstrated strong agreement with the computed stability boundaries.

Given the infinite-dimensional nature of the underlying delay differential equations, coupled with the complexities introduced by hysteresis and scalable damping effects, the system exhibits complex dynamical behavior. This study opens new opportunities for further research, particularly in refining approximation methods, extending stability criteria, and exploring additional nonlinear interactions within such coupled systems. Future work may also focus on experimental validation and real-world implementation of these theoretical findings to enhance the practical applicability of TMD systems in engineering applications.

Acknowledgements. The authors would like to sincerely thank Aman Gautam, for his assistance during the course of this research.

Declarations

The authors declared no potential conflicts of interest with respect to the research, authorship, and/or publication of this article.

References

[1] Wittenmark B, Nilsson J, Torngren M. Timing problems in real-time control systems. In *Proceedings of 1995 American Control Conference-ACC'*95 1995 Jun 21 (Vol. 3, pp. 2000-2004). IEEE.

[2] Sipahi R, Niculescu SI, Abdallah CT, Michiels W, Gu K. Stability and stabilization of systems with time delay. *IEEE Control Systems Magazine*. 2011 Jan 13; 31(1):38-65.

[3] Stepan G. Retarded Dynamical Systems: Stability and Characteristic Functions. *Longman Scientific & Technical*, 1989.

[4] Hale JK. *Theory of Functional Differential Equations*. Springer-Verlag, 1977.

[5] Engelborghs K, Luzyanina T, Samaey G. DDE-BIFTOOL: a Matlab package for bifurcation analysis of delay differential equations. *TW Repor*t. 2000 May; 305(1).

[6] Bellen A, Zennaro M. Numerical solution of delay differential equations by uniform corrections to an implicit Runge-Kutta method. *Numerische Mathematik*. 1985 Jun; 47:301-16.

[7] Atay FM. *Complex Time-Delay Systems*. Springer, 2010.

[8] Michiels W, Niculescu SI. Stability, Control, and Computation for Time-Delay Systems: An Eigenvalue-Based Approach. *SIAM*, 2014.

[9] Balija SK, Biswas S, Chatterjee A. Stability aspects of the Hayes delay differential equation with scalable hysteresis. *Nonlinear Dynamics*. 2018 Aug;93:1377-93.

[10] Ospanov A. Delay Differential Equations and Their Application to Micro Electro Mechanical Systems.

[11] Insperger T, Stepan G. Semi-Discretization for Time-Delay Systems: Stability and Engineering Applications. *Springer*, 2011.

[12] Frahm, H. (1911). Device for Damping Vibrations of Bodies. *U.S. Patent No. 989*,958.

[13] Den Hartog, J.P. (1956). *Mechanical Vibrations*. McGraw-Hill.

[14] Zuo L. Effective and robust vibration control using series multiple tuned-mass dampers.

[15] Gu M. Control of wind-induced vibration of long-span bridges and tall buildings. *Frontiers of Architecture and Civil Engineering in China*. 2007

Feb;1:51-62.

[16] Li, C, & Li, H.N. (2016). Hybrid Tuned Mass Damper Systems for Vibration Control in Buildings. *Structural Control and Health Monitoring*, 23(9), 1132-1147.

[17] Lu, Z, Yang, J, & Zhou, Y. (2021). Semi-Active Tuned Mass Damper with Magnetorheological Damper for Bridge Vibration Control. *Journal of Bridge Engineering*, 26(4), 04021003.

[18] Jian, J., & Ou, J. (2016). Delay Compensation in Active Tuned Mass Dampers Using Predictive Control Algorithms. *Structural Control and Health Monitoring*, 23(12), 1429-1443.

[19] Zhao X, et al. Stability Analysis of Semi-Active Tuned Mass Damper Systems with Delays. *Journal of Sound and Vibration*. 2018.

[20] Gebrial B, Sinan MM. Mass ratio factor for optimum tuned mass damper strategies. *International Journal of Mechanical Science*, 2013 Jun;68-84.

[21] Rowett FE. Elastic hysteresis in steel. *Proceedings of the Royal Society of London*. Series A, Containing Papers of a Mathematical and Physical Character. 1914 Mar 2;89(614):528-43.

[22] Preisach F. Über die magnetische Nachwirkung. *Zeitschrift für Physik*. 1935.

[23] Iwan WD. A Distributed-Element Model for Hysteresis and Its Application to Harmonic Vibration. *Journal of Applied Mechanics*. 1966.

[24] Bouc R. Forced Vibrations of Mechanical Systems with Hysteresis. *Comptes Rendus de l'Académie des Sciences*. 1967.

[25] Wen YK. Method for Random Vibration of Hysteretic Systems. *Journal of Engineering Mechanics*. 1976.

[26] Biswas S, Jana P, Chatterjee A. Hysteretic damping in an elastic body with frictional microcracks. *International Journal of Mechanical Sciences*. 2016 Apr 1;108:61-71.

[27] Rathore KK, Biswas S. Multi-frequency Approximation for a Hysteretically Damped Tuned Mass System. In *Recent Trends in Mechanical Engineering: Select Proceedings of PRIME* 2021-2023 Jun 8 (pp. 99-107). Singapore: Springer Nature Singapore.

[28] Rathore KK, Biswas S. Tuned mass systems with the Bouc-Wen and a hybrid hysteresis. *Noise & Vibration Worldwide*. 2022 Jul;53(7-8):366-76.

[29] Rathore KK, Biswas S. A Versatile Asymmetric Hysteresis Model Motivated by a Study of Elastic Material with Microcracks. *Journal of Vibration Engineering & Technologies*. 2024 Jan;12(1):279-93.

[30] Berardengo M, Cigada A, Guanziroli F, Manzoni S. An adaptive tuned mass damper based on shape memory alloys with an extended range of frequency. In2014 IEEE Workshop on Environmental, *Energy, and Structural Monitoring Systems Proceedings* 2014 Sep 17 (pp. 1-6). IEEE.

[31] Ma W, Yang Y, Yu J. General routine of suppressing single vibration mode by multi-DOF tuned mass damper: application of three-DOF. *Mechanical Systems and Signal Processing*. 2019 Apr 15;121:77-96.

[32] Rana, R, & Soong, T T (1998). Parametric Study and Simplified Design of Tuned Mass Dampers. *Engineering Structures*, 20(3), 193-204.

[33] Mathis, A. T., Balaji, N. N., Kuether, R. J., Brink, A. R., Brake, M. R., Quinn, D.D., 2020, A review of damping models for structures with mechanical joints, *Applied Mechanics Reviews*, 72(4).

[34] Skelton RP, Maier HJ, Christ HJ. The Bauschinger effect, Masing model and the Ramberg?Osgood relation for cyclic deformation in metals. Materials Science and Engineering: A. 1997 Nov 15;238(2):377-90.

[35] Ibarra LF, Medina RA, Krawinkler H. Hysteretic models that incorporate strength and stiffness deterioration. Earthquake engineering & structural dynamics. 2005 Oct;34(12):1489-511.

[36] Hassani V, Tjahjowidodo T, Do TN. A survey on hysteresis modeling, identification and control. Mechanical systems and signal processing. 2014 Dec 20;49(1-2):209-33.

[37] Yang, Y.B., & Lin, S. (2018). "A Modified Bouc-Wen Model for Hysteretic Behavior in Seismic Isolation Systems." Journal of Structural Engineering, 144(9), 04018167.

[38] Wahi P. A study of delay differential equations with applications to machine tool vibrations (Doctoral dissertation, Ph. D. Thesis, Indian Institute of Science, Bangalore).

[39] Maiti S, Bandyopadhyay R, Chatterjee A. Vibrations of an Euler-Bernoulli beam with hysteretic damping arising from dispersed frictional microcracks. Journal of Sound and Vibration. 2018 Jan 6;412:287-308.